

Microstructures of Niobium Components Fabricated by Electron Beam Melting

Edwin Martinez · Lawrence E. Murr · Jennifer Hernandez · Xuemin Pan ·
Krista Amato · Pedro Frigola · Cesar Terrazas · Sara Gaytan · Emmanuel Rodriguez ·
Francisco Medina · Ryan B. Wicker

Received: 1 March 2013/Revised: 26 March 2013/Accepted: 25 April 2013/Published online: 11 May 2013
© Springer Science+Business Media New York and ASM International 2013

Abstract This article presents columnar grain structures characteristic of niobium components fabricated by electron beam melting, using two different size and size distribution spherical powders produced by rapid solidification atomization. The precursor powder microstructures are characterized by equiaxed grains while the columnar grain structure in the electron beam melted (EBM)-fabricated products contain dislocation substructures ranging in density from $\sim 10^9$ to $10^{10}/\text{cm}^2$ as observed by transmission electron microscopy. X-ray diffraction analysis illustrates the variations in orientations in both the precursor powders and the fabricated components. Microindentation hardness values ranged from 0.8 GPa for the precursor powders and 1.1 and 0.92 GPa for the EBM-fabricated, solid components.

Keywords Electron beam melting · Niobium · Light microscopy · Electron microscopy

Introduction

Charged particle accelerators utilize superconducting radio frequency (SRF) resonant cavity devices to obtain extremely high quality factors which store energy with very low loss and correspondingly narrow bandwidth. Particle acceleration occurs on passing through apertures in such cavities which are driven by resonant frequencies between 0.2 to 3 GHz. A common SRF niobium (Nb) cavity operating at 1.3 GHz at <2 K can produce a quality factor, $Q \cong 5 \times 10^{10}$. Nb, the highest superconducting transition metal (~ 7.5 K) has been the material of choice in cavity production, but it has posed considerable challenges in their manufacture, including irregular mechanical response of Nb sheet in deep drawing and welding operations. Good formability is required to produce complex shapes with requisite surface quality required for optimal high frequency performance. Jiang et al. [1] and Agrew et al. [2] have noted that microstructure irregularities, including grain size banding and large local texture gradients contributed to the irregular mechanical behavior of Nb. Hartwing et al. [3] used equal channel angular extrusion on bars prior to sheet rolling to produce a refined microstructure in Nb.

In the present study, we conducted a preliminary assessment of the prospects for fabricating simple Nb geometries by electron beam melting (EBM). EBM has the ability to form very complex components from precursor powder material by successive and selective layer melting using computer-aided design software to direct and control the electron beam [4–6]. The problems faced in the EBM processing of Nb powder is the latter's very high melting point of approximately 2495 °C, and the difficulty in realizing the efficient coupling of the beam energy to the powder layer and the corresponding powder size and size distribution.

E. Martinez (✉) · L. E. Murr · J. Hernandez · K. Amato
Department of Metallurgical and Materials Engineering, The
University of Texas at El Paso, El Paso, TX 79968, USA
e-mail: emartinez21@miners.utep.edu

X. Pan
School of Materials Science and Engineering, Dalian University
of Technology, Dalian 116024, Liaoning, China

P. Frigola
Radiabeam Technologies, Santa Monica, CA 90404, USA

C. Terrazas · S. Gaytan · E. Rodriguez · F. Medina ·
R. B. Wicker
W.M. Keck Center for 3D Innovation, The University of Texas
at El Paso, El Paso, TX 79968, USA

The microstructures of the Nb powders used in this study were examined by light microscopy (LM), scanning electron microscopy (SEM), and x-ray diffraction (XRD). The as-built EBM components were examined by LM, SEM, XRD, and transmission electron microscopy (TEM). Microindentation hardness measurements were made on the precursor powders and the EBM-fabricated components for comparison.

The aim of this study was to demonstrate the fabrication of metal components for high-temperature applications in a modified EBM system. Nb was the first material ever tested on this system; a significant amount of experimentation and process optimization was required to produce an acceptable build. Bimodal powders as well as uniformly sized powders were used in this study to determine how particle size would affect the densification of the as-built product.

Experimental Procedures

Plasma-atomized, rapidly solidified Nb powders were utilized in two forms: a uniformly sized spherical powder as illustrated in Fig. 1, with an average particle diameter of

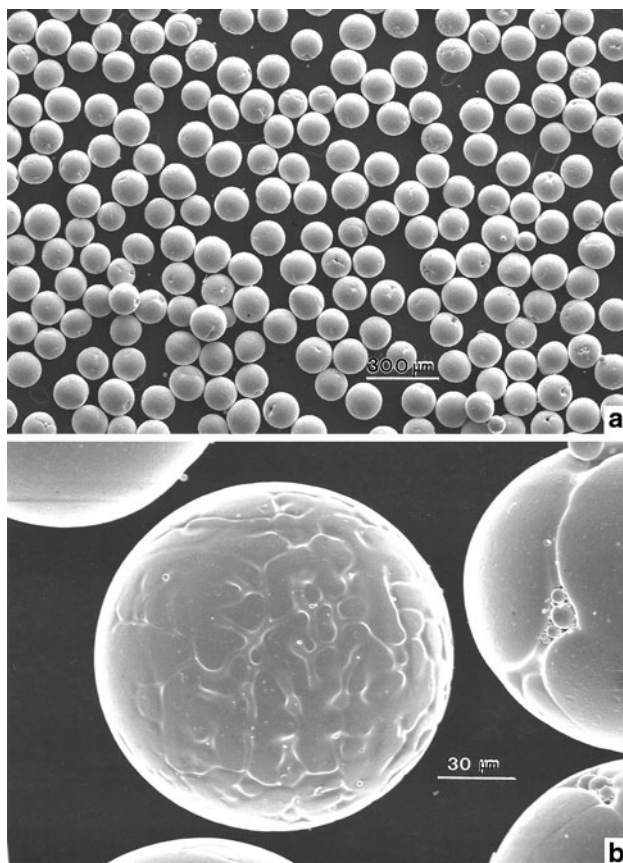


Fig. 1 Nb-atomized, unisize precursor powder. (a) Low-magnification SEM image. (b) High-magnification SEM image

130 μm , and a bimodal spherical powder as illustrated in Fig. 2, with average particle diameters of 43 and 86 μm . Spherical powders were used selected because of their improved flow properties compared to irregularly shaped powders.

The Nb powders shown in Figs. 1 and 2 were processed in an S-12 Arcam EBM system modified for high-temperature applications. The modifications included an air-cooled electron gun with an insulating space between the gun and the build chamber. The system also included additional heat shields to decrease heat loss by the building components. The start plate was at a temperature of ~ 720 $^{\circ}\text{C}$; this temperature was determined through empirical studies and was selected to promote sintering of the powder underneath the plate, to prevent it from shifting during the build process. When the start plate reached about ~ 720 $^{\circ}\text{C}$, the system was stopped manually and allowed to cool to ~ 580 $^{\circ}\text{C}$ to prevent agglomeration of the powders; agglomeration was a significant problem during initial builds of with Nb. After it cooled down to ~ 580 $^{\circ}\text{C}$, the system was initiated again with preheat scans of successive layers utilizing a scan speed of $\sim 10^3$ mm/s and a beam current of ~ 2 mA. These

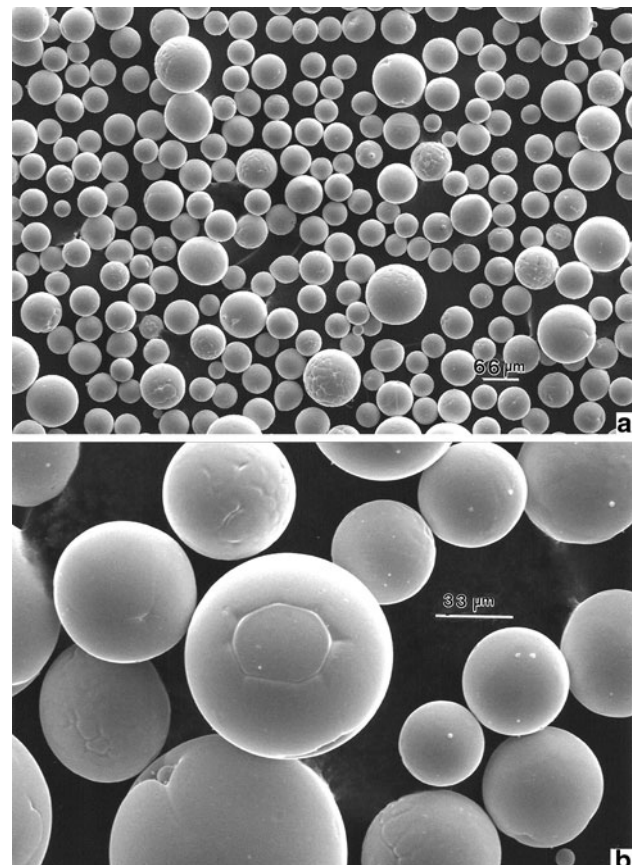


Fig. 2 Nb-atomized bimodal-sized precursor powder. (a) Low-magnification SEM image. (b) High-magnification SEM image

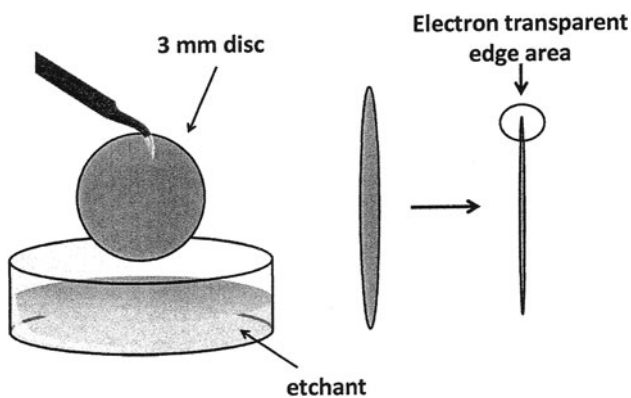


Fig. 3 Schematic view illustrating chemical thinning of 3-mm disks for TEM observation

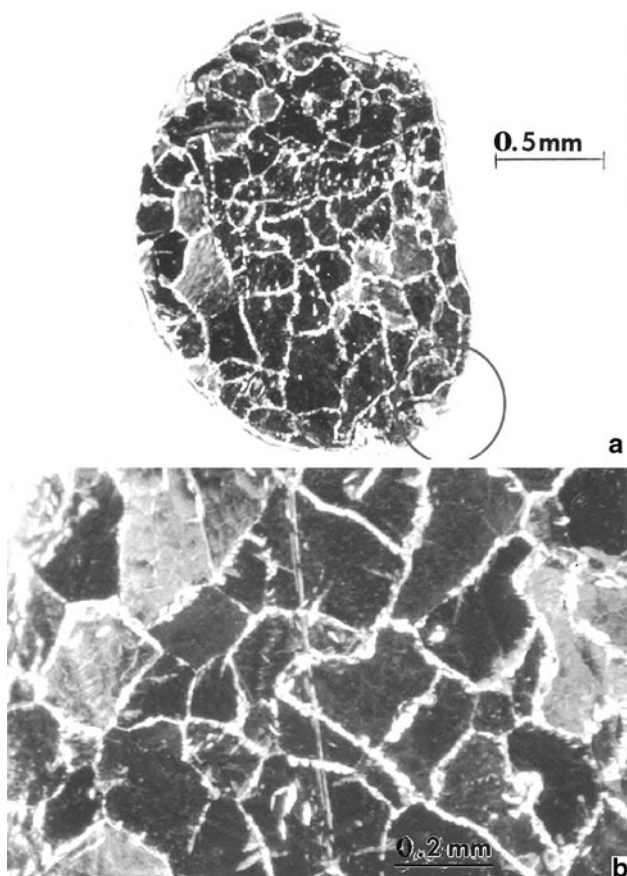


Fig. 4 LM views of chemically thinned Nb TEM sample showing electron transparent area circled (a). (b) shows a magnified view exhibiting grain structure which exists in the EBM-fabricated component plane *perpendicular* to the build direction

conditions produced a preheat temperature, created by the e-beam, of ~ 610 °C. A delay was included in the build program which would reduce the temperature to ~ 580 °C and raise it back up to ~ 610 °C throughout the build process (note that this is not the standard build process for

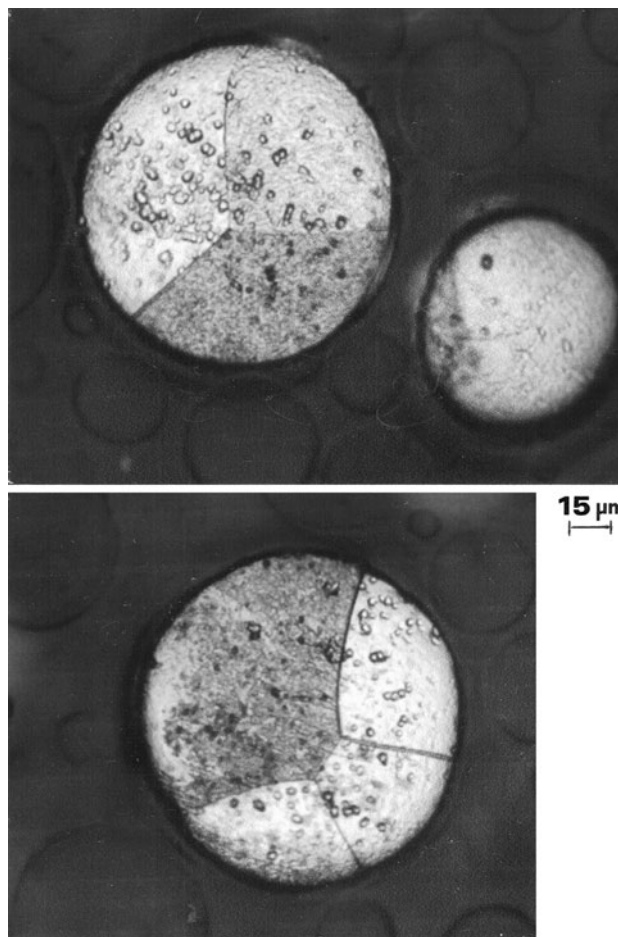


Fig. 5 Bimodal size Nb precursor powder interior structure observed by LM

materials in this instrument). The periodic decrease in temperature was required to prevent powder agglomeration which would have resulted in an inconsistent powder surface during the powder raking step. The melt scan speed ranged from ~ 250 to 300 mm/s at a beam current of 12 mA. The system was operated in a vacuum of $\sim 10^{-5}$ Torr, and the electron gun accelerating voltage was 60 kV. The details of the EBM system, including powder layer-raking process, have been described in detail elsewhere [4–6].

Fabricated components measuring ~ 3.8 cm in diameter and 1.5 cm in height were cut into smaller coupons, which were embedded in a hard epoxy mount in orientations both perpendicular and parallel to the build direction; these samples are designated horizontal (H) and vertical (V), respectively. These mounted samples were ground, polished, and etched for LM examination.

The uniformly sized powder (Fig. 1) component samples were etched in a 1:4 solution of HF:HNO₃, while the bimodal powder component samples were etched in a solution consisting of 30 mL HCl, 15 mL HNO₃, and

30 mL HF. Different etchants were chosen to obtain sufficient contrast in each sample. The etched samples were examined in a light metallograph equipped with a digital imaging system. In addition, powder samples (Figs. 1, 2) were embedded in epoxy and ground to reveal the powder particle interiors and then polished and etched as indicated for the fabricated products. Vickers microindentation testing was performed on both the etched fabricated samples and the powder samples; at least, 20 measurements for each sample were recorded, and the averages were determined for comparison.

Samples, as illustrated in Figs. 1 and 2, were examined by SEM using secondary electron imaging in a field emission SEM operated at 20 kV accelerating potential; compositional analysis was performed using an energy-dispersive x-ray spectrometer.

XRD utilizing a Cu ($K\alpha$) x-ray source was performed on the precursor powders (Figs. 1, 2) as well as the as-fabricated specimen sections cut from the EBM component products. These sections were referred to as horizontal and vertical plane sections consistent with LM observations described above.

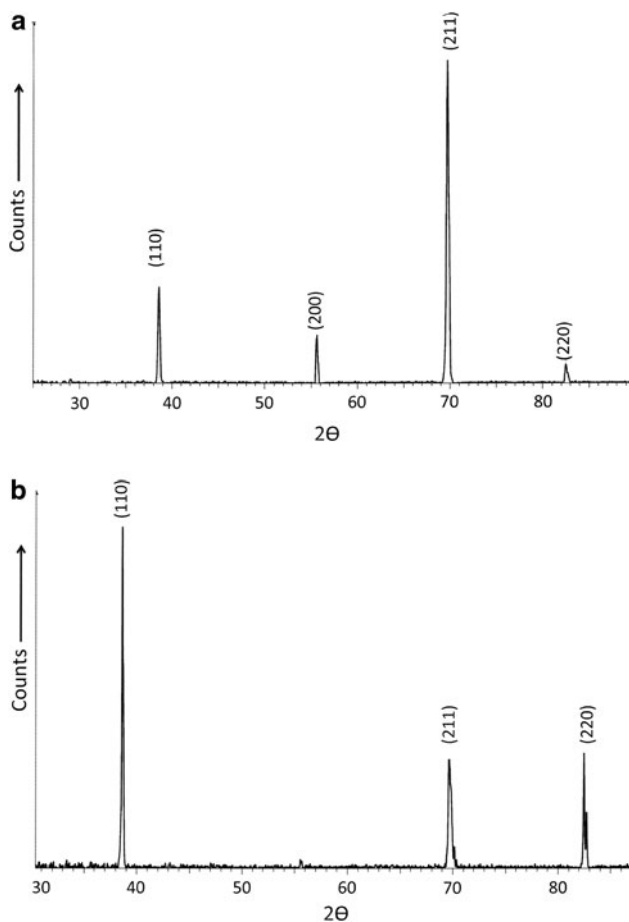


Fig. 6 XRD spectra for atomized Nb precursor powders. (a) Unisize powder (Fig. 1). (b) Bimodal powder (Fig. 2)

Thin sections were cut from the horizontal and vertical reference coupons extracted from EBM-fabricated components and ground to a thickness of ~ 0.2 mm. Standard 3-mm disks for TEM were then punched from these thin sections. These punched disks were dipped with plastic coated stainless steel tweezers into an etching solution consisting of 70% HNO_3 and 30% HF to which a few drops of HCl were added when the sample thinned as illustrated schematically in Fig. 3. While the sample diameter and thickness were reduced in this chemical etching process, the edges thinned more rapidly and produced irregular, electron transparent sections as illustrated in Fig. 4(a). This etching also revealed the grain structures associated with the EBM-fabricated components as shown in Fig. 4(a) and the magnified section view shown in Fig. 4(b). The chemically etched disk sections shown in Fig. 4(a) were observed in a high-resolution TEM operated at 300 kV accelerating voltage.

Results and Discussion

Figure 5 shows select examples of the interior Nb powder particle microstructure for the bimodal powder illustrated in Fig. 2(b); these images are also characteristic of the uniform particle size powder in Fig. 1(b). The microstructure consisted of equiaxed grains. Figure 6 shows the corresponding XRD spectra for the Nb powder represented

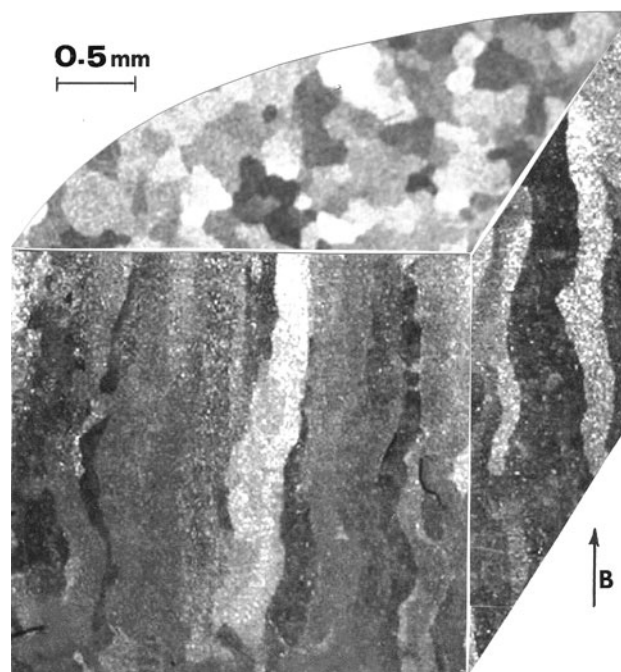


Fig. 7 3D-LM image composite showing columnar grain structure in EBM-fabricated component from unisize precursor powder (Fig. 1). Arrow at lower right indicates the build (*B*) direction

by Figs. 1(a) and 2(a), and illustrates the bcc structure with a lattice parameter of $a = 0.33 \text{ nm}$.

Figure 7 shows a LM, 3D image composition representing a section of an EBM-fabricated component using the uniform Nb precursor powder (Fig. 1) The microstructure consists of columnar grains producing an equiaxed grain structure with a grain size of $\sim 200 \mu\text{m}$ in the horizontal reference plane perpendicular to the build direction marked B in Fig. 7. There is recognizable porosity, especially in the vertical reference plane, illustrating the columnar grains in Fig. 7. Figure 8 shows representative XRD data characteristic of the horizontal and vertical reference planes represented in Fig. 7, and illustrating some preferred orientations which, as shown by the gray-scale grain contrast especially in the horizontal reference plane in Fig. 7, shows a mixture of at least five orientations.

Figure 9 shows a representative TEM bright-field image in the horizontal reference plane in Fig. 7, which illustrates predominantly screw dislocations in a (111) grain surface orientation, as shown by the selected-area electron diffraction (SAED) pattern insert. The operating reflection is $[\bar{1}10]$ as shown by the circled diffraction spot next to the beam stop in Fig. 9.

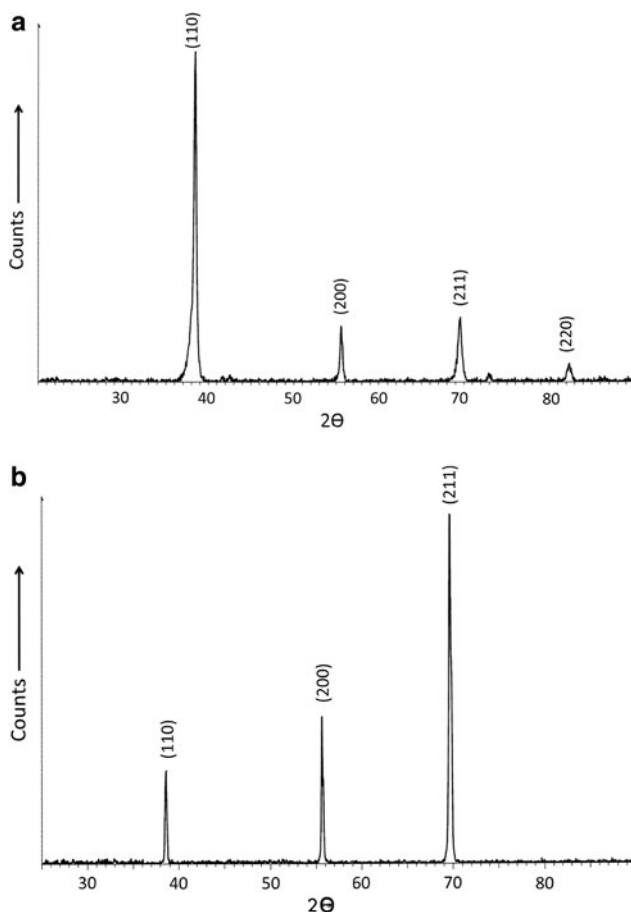


Fig. 8 XRD spectra representing the horizontal (a) and vertical (b) reference planes illustrated in Fig. 7

Figure 10 shows a 3D-LM image construction representing a section from an EBM-fabricated component using the bimodal Nb powder distribution represented by Fig. 2. In contrast to Fig. 7, there is no recognizable porosity, and the build is considerably more optimized. The XRD spectra corresponding to Fig. 10 were similar to those shown in Fig. 8 with the exception of stronger (200) and (110) peaks in the horizontal and vertical reference planes, respectively. Figures 11 and 12 illustrate dislocation microstructures represented by these corresponding orientations in the horizontal (H) and vertical (V) reference planes, respectively, in Fig. 10. Figure 12 also illustrates a triple junction of low-angle grain boundaries.

It should be noted that, when comparing the dislocation substructures illustrated in Figs. 9, 11, and 12, there are no dislocation cell structures characteristic of Nb wrought and rolled plate and sheet products. Dislocation densities were measured from the relationship [7]:

$$\rho \cong 2N / \sum L(t), \tag{1}$$

where a random grid line transparency was superimposed on TEM micrographs, including Figs. 9, 11, and 12. The intersections of dislocation lines with the grid lines are denoted as N in Eq 1, while the total grid line length is

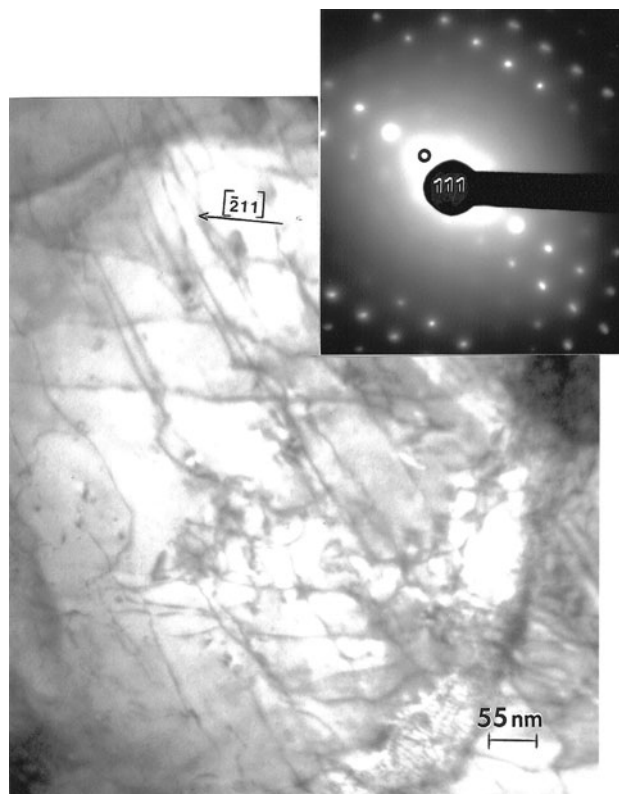


Fig. 9 TEM bright-field image showing dislocation structures in the horizontal reference plane in Fig. 7. The (111) plane surface orientation is indicated in the SAED pattern insert

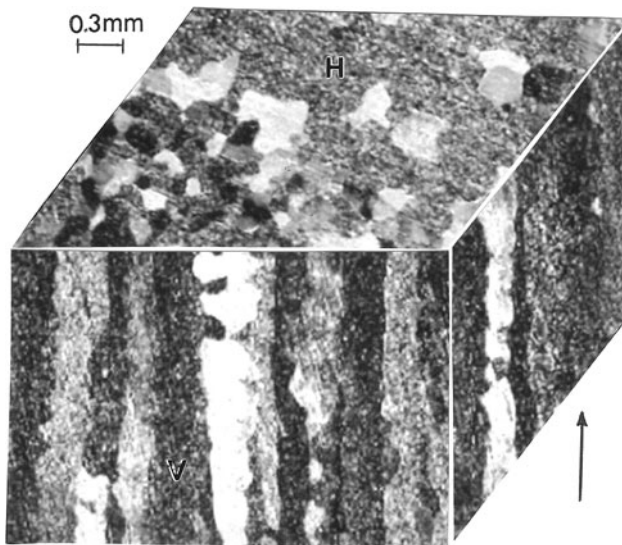


Fig. 10 3D-LM image composite showing columnar grain structure in EBM-fabricated component from bimodal precursor powder (Fig. 2). Arrow indicates the EBM build direction. Horizontal and vertical reference planes are denoted *H* and *V*, respectively

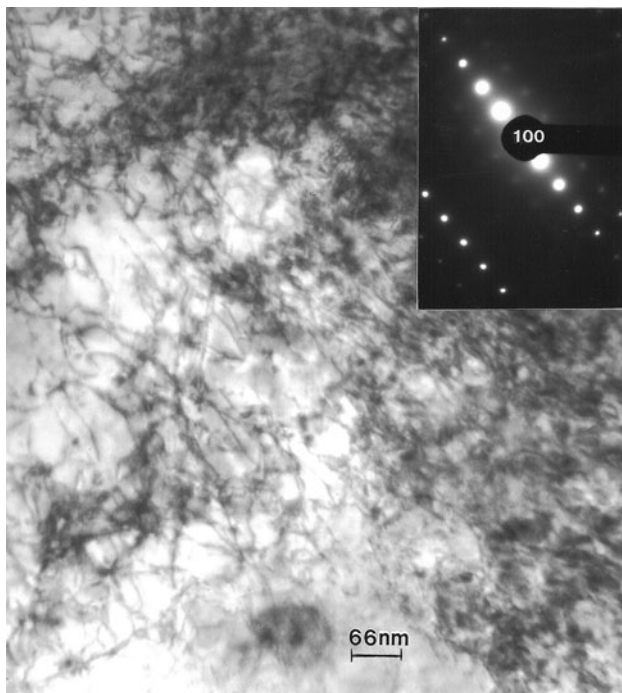


Fig. 11 TEM bright-field image representing dislocation structures in a (100) oriented grain in the horizontal (*H*) reference plane in Fig. 10. The SAED pattern *inset* shows the (100) orientation

denoted $\sum L$. The average film thickness, t , in Eq 1 was taken as 0.3 μm , following the earlier TEM analysis on Nb by Conrad et al. [8]. This is a reasonable thickness considering the material at the operating potential in the TEM, 300 kV. Dislocation densities varied from $\sim 10^9/\text{cm}^2$ as

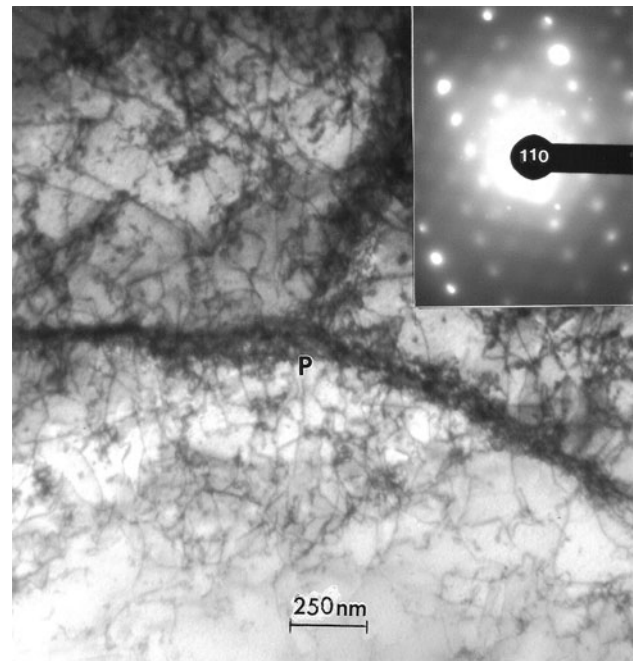


Fig. 12 TEM bright-field image representing dislocation structures in a (110) oriented grain in the vertical (*V*) reference plane in Fig. 10. The SAED pattern *inset* shows the (110) orientation. Extra diffraction spots arise from the low-angle grains characterized by boundaries meeting at the triple point at *P*

shown in Fig. 9 to $\sim 10^{10}/\text{cm}^2$ as shown in Figs. 11 and 12. These values are one to two orders of magnitude higher than prior observations in unstrained Nb sheet specimens having grain sizes ranging from 32 to 435 μm [8]. However, straining of the 32 μm grain size material to 4% produced a dislocation density of $\sim 10^{10}/\text{cm}^2$ [8].

Measurement of the microindentation hardness for the Nb precursor powders produced average values of 0.8 GPa, while the EBM-fabricated components from uniform powder (Fig. 1) and represented by Fig. 7 produced average microindentation hardness values of 1.1 GPa. For the bimodal powder products represented by Fig. 10, the average microindentation hardness was 0.92 GPa. These values are much higher than annealed Nb sheet, where the microindentation hardness ranged from 0.3 to 0.13 GPa for grain sizes ranging from 32 μm to 435 μm , respectively [8].

Conclusions

For the first time, Nb components have been fabricated by electron beam melting. The process to build such components proved difficult, but after creating a unique delay in the build process, satisfactory results were obtained. Optimized solid components were fabricated from a bimodal precursor powder having an average grain size of $\sim 65 \mu\text{m}$. The

bimodal powder is preferred for manufacturing components by EBM because the smaller powder particles can fill the interstitial volumes between the larger powder particles, therefore creating a denser component. The build conditions for the Nb were selected specifically to stop the powders from agglomerating and to allow the powder rake in the system to more effectively smoothen the powder bed. The EBM-fabricated components exhibited a columnar grain structure parallel to the EBM build direction. Dislocation substructures exhibited densities ranging from 10^9 to $10^{10}/\text{cm}^2$, with no cell structure. In the future, the ability to manufacture Nb components by EBM may lead to improved fabrication of complex superconducting components.

Acknowledgments This research was supported in part by Mr. and Mrs. Mac Intosh Murchison Endowed Chairs.

References

1. H. Jiang, T.R. Bieler, C. Compton, T.C. Grimm, Evaluation of recrystallization textures from cold rolling textures with reversed rolling in high purity niobium. *TMS Lett.* **1**(8), 177–178 (2004)
2. S.R. Agnew, F. Zeng, G.R. Myneni, Ultrasonic velocity and texture of high RRR niobium. *Mater. Tech.* **7–8**, 38–44 (2003)
3. K.T. Hartwig, J. Wang, D.C. Baars, T.R. Bieler, S.N. Mathaudhu, R.E. Barber, Microstructural retirement of niobium for superconducting RF cavities. *IEEE Trans. Appl. Supercond.* **17**(2), 1305–1309 (2007)
4. L.E. Murr, E. Martinez, S.M. Gaytan, D.A. Ramirez, J. Hernandez, Contributions of light microscopy to contemporary materials characterization : the new directional solidification. *Metallogr. Microstruct. Anal.* **1**, 45–58 (2012)
5. L.E. Murr, E. Martinez, S.M. Gaytan, D.A. Ramirez, J. Hernandez, K.N. Amato, P.W. Shindo, F.R. Medina, R.B. Wicker, Metal fabrication by additive manufacturing using laser and electron beam melting technologies. *J. Mater. Sci. Technol.* **28**(1), 1–14 (2012)
6. L.E. Murr, E. Martinez, K.H. Amato, S.M. Gaytan, J. Hernandez, D.A. Ramirez, P.W. Shindo, F. Medina, R.B. Wicker, Fabrication of metal and alloy components by additive manufacturing : examples of 3D materials science. *J. Mater. Res. Technol.* **1**(1), 24–54 (2012)
7. L.E. Murr, *Electron and Ion Microscopy and Microanalysis* (Marcel Dekker, New York, 1990)
8. H. Conrad, S. Feuerstein, L. Rice, Effects of grain size on the dislocation density and flow stress of niobium. *Mater. Sci. Eng.* **2**, 157–168 (1967)